Ore Geology Reviews 90 (2017) 274–286

Contents lists available at ScienceDirect

Ore Geology Reviews

journal homepage: www.elsevier.com/locate/oregeo

The role of silica in the hydrous metamorphism of chromite

Vanessa Colás [a,*], José Alberto Padrón-Navarta [b], José María González-Jiménez [c], Isabel Fanlo [d], Vicente López Sánchez-Vizcaíno [e], Fernado Gervilla [c], Ricardo Castroviejo [f]

[a] Instituto de Geología, Universidad Nacional Autónoma de México, Ciudad Universitaria, 04510 Ciudad de México, Mexico
[b] Géosciences Montpellier, CNRS & Univ. Montpellier (UMR5243), 34095 Montpellier, France
[c] Departamento de Mineralogía y Petrología, Universidad de Granada, Facultad de Ciencias, Avda. Fuentenueva s/n, 18002 Granada, Spain
[d] Departamento de Ciencias de la Tierra, Universidad de Zaragoza, Pedro Cerbuna 12, 50009 Zaragoza, Spain
[e] Departamento de Geología, Universidad de Jaén, Escuela Politécnica Superior, Avda. de la Universidad s/n, 23700 Linares, Spain
[f] E.T.S. Ing. Minas y Energía, Universidad Politécnica de Madrid, Ríos Rosas 21, 28003 Madrid, Spain

ARTICLE INFO

Article history:
Received 27 June 2016
Received in revised form 8 February 2017
Accepted 15 February 2017
Available online 2 March 2017

Keywords:
Chromite
Metamorphism
SiO_2-rich fluids
Open system model
Tapo Ultramafic Massif

ABSTRACT

Retrograde hydrous metamorphism has produced three types of microstructures in chromite grains from chromitites and enclosing rocks of the Tapo Ultramafic Massif (Central Peruvian Andes). In semi-massive chromitites (60–80 vol% chromite), (i) *partly altered chromite* with homogeneous cores surrounded by lower Al_2O_3 and MgO but higher Cr_2O_3 and FeO porous chromite with chlorite filling the pores. In serpentinites (ii) *zoned chromite* with homogeneous cores surrounded by extremely higher Fe_2O_3 non-porous chromite and magnetite rims, and (iii) *non-porous chromite* grains. The different patterns of zoning in chromite grains are the consequences of the infiltration of reducing and SiO_2-rich fluids and the subsequent heterogeneous interaction with more oxidizing and Fe-bearing fluids. During the first stage of alteration under reduced conditions magmatic chromite is dissolved meanwhile new metamorphogenic porous chromite crystallizes in equilibrium with chlorite. This reaction that involves dissolution and precipitation of minerals is here modeled thermodynamically for the first time. μSiO_2-μMgO pseudosection calculated for unaltered semi-massive chromitites at 2 kbar and 300 °C, the lowest P-T conditions inferred from the Tapo Ultramafic Massif and Marañón Complex, predicts that chromite + chlorite (i.e., partly altered chromite) is stable instead of chromite + chlorite + brucite at progressive higher μSiO_2 but lower μMgO. Our observation is twofold as it reveals that the important role of SiO_2 and MgO and the open-nature of this process. P-T-X diagrams computed using the different P-T pathways estimated for the enclosing Tapo Ultramafic Massif reproduce well the partial equilibrium sequence of mineral assemblages preserved in the chromitites. Nevertheless, it is restricted only to the P-T conditions of the metamorphic peak and that of the latest overprint. Our estimations reveal that a high fluid/rock ratio (1:40 ratio) is required to produce the microstructures and compositional changes observed in the chromitites from the Tapo Ultramafic Massif. The circulation of SiO_2-rich fluids and the mobilization of MgO from the chromitite bodies are linked with the formation of garnet amphibolites and carbonate-silica hydrothermalites (i.e., listwaenites and birbirites) in the ultramafic massif. The origin of these fluids is interpreted as a result of the dissolution of orthopyroxene and/or olivine from the metaharzburgites and metagabbros enclosed in the Tapo Ultramafic Massif.

1. Introduction

Chromite grains often exhibit complex patterns of zoning related with hydrous or thermal metamorphism (Loferski, 1986; Evans and Frost, 1975; Kimball, 1990; Fleet et al., 1993; Abzalov, 1998; Barnes, 2000; Proenza et al., 2004; González-Jiménez et al., 2009; González-Jiménez et al., 2015, 2016; Merlini et al., 2009; Mukherjee et al., 2010; Mukherjee et al., 2015; Gervilla et al., 2012; Saumur and Hattori, 2013; Colás et al., 2014; Evans, 2015). The development of the zoning depends on many factors, including the composition and size of chromite grains, the texture of chromitite bodies, the pressure and temperature conditions of the metamorphism, the deformation and fluid/rock ratios, as well as intrinsic thermodynamic parameters of the metamorphic fluid

* Corresponding author at: Instituto de Geología, Universidad Nacional Autónoma de México, Ciudad Universitaria, 04510 Ciudad de México, Mexico.
E-mail address: vcolas86@gmail.com (V. Colás).

http://dx.doi.org/10.1016/j.oregeorev.2017.02.025
0169-1368/

such as oxygen fugacity (fO_2), content of CO_2 (XCO_2) and silica activity ($aSiO_2$) (Bliss and MacLean, 1975; Evans and Frost, 1975; Loferski, 1986; Candia and Gaspar, 1997; Barnes, 2000; Proenza et al., 2004; Merlini et al., 2009; Barra et al., 2014; Evans, 2015; Satsukawa et al., 2015).

Previous estimations of the temperatures for the alteration of ophiolitic chromitites during hydrous metamorphism using thermodynamic models indicate that the alteration of chromite takes place under water-saturated conditions below 700 °C and variable pressure (up to ca. 10 kbar) (Gervilla et al., 2012; Barra et al., 2014; González-Jiménez et al., 2015, 2016). Under these P-T conditions that are typical of the amphibolite-facies and greenschist-facies metamorphism, isochemical phase diagrams (or pseudosections) predict that the stable assemblage is chlorite + chromite + brucite + (diaspore) (Gervilla et al., 2012; Barra et al., 2014; González-Jiménez et al., 2015, 2016). However, brucite is commonly absent in many chromite-bearing serpentinized rocks (Ulmer, 1974; Evans and Frost, 1975; Oze et al., 2004; Polat et al., 2006; Gargiulo et al., 2013; Gahlan et al., 2015; Evans, 2015; Kotschoubey et al., 2016) or metamorphosed chromitites elsewhere (Zaccarini et al., 2008; Akmaz et al., 2014; Colás et al., 2014; Mukherjee et al., 2015). Frost and Beard (2007), Jöns et al. (2010) and Frost et al. (2013) showed that the stability of brucite during serpentinization might not only depend on pressure and temperature, but also strongly on the infiltration of silica-rich fluids. This implies that the hydrous metamorphism of chromitites should take place under open system condition relative to SiO_2 (i.e., SiO_2 dissolved in fluids), which would cause significant changes in the mineral assemblage of altered chromitite bodies.

In this work we apply a new thermodynamic approach able to explain the absence of brucite in metamorphosed chromitites. The refined thermodynamic model takes into account that alteration of chromite during metamorphism is dominated by dissolution-precipitation in an open system saturated in fluids. The case study of the Tapo Ultramafic Massif (Eastern Cordillera, Perú) is taken to evaluate our model because it contains chromitite bodies metamorphosed from eclogite- or amphibolite-facies to greenschist-facies, which allows us to assess the compositional variations of metamorphic chromite as a possible fingerprint of P-T pathways. We calculate μSiO_2-μMgO and P-T-X pseudosections in order to reproduce the phase relation changes that hydrous metamorphism has produced on the chromitite bodies and their forming chromite grains. This approach is carried out by contrasting different P-T pathways estimated for metamorphic rocks enclosing the chromite-bearing ultramafic massif. Our results help to better decode the processes of metamorphism of ophiolitic chromitites unravelling the true nature of the fluids involved in such processes.

2. Geological background

The Tapo Ultramafic Massif is a metamorphosed ophiolitic ultramafic massif exposed in the Eastern Cordillera of the Central Peruvian Andes (Castroviejo et al., 2009; Tassinari et al., 2011; Willner et al., 2014). It is part of the metamorphic basement of the Eastern Cordillera, known as Marañón Complex (Wilson and Reyes, 1964; Dalmayrac et al., 1980) or Huacár Group (Megard et al., 1996) (Fig. 1), and mainly consists of strongly tectonized and highly serpentinized metaharzburgites and minor metadunites (Tassinari et al., 2011) that enclose chromitite bodies, banded metagabbros, lenses of garnet amphibolites and rodingites (Tassinari et al., 2011; Willner et al., 2014). Silica and carbonate-silica hydrothermalites, birbirites and listwaenites, are present along thrusts and faults crosscutting the ultramafic massif. The Tapo Ultramafic Massif is unconformably overlain by fossiliferous Lower Carboniferous and Upper Permian sedimentary rocks (Ambo and Mitú Groups; Dalmayrac et al., 1980), which are overlain by an Upper Triassic-Lower Jurassic carbonate sequence (Pucará Group) (Fig. 1). Further details on the geology of the Tapo Ultramafic Massif can be found in the works of Castroviejo et al. (2009), Tassinari et al. (2011) and Willner et al. (2014).

Willner et al. (2014) performed P-T pseudosections based on mineral assemblages from garnet-bearing amphibolites of the Tapo Ultramafic Massif and from a suite of enclosing metamorphic rocks (metabasites and metapelites of the Marañón Complex), estimating a high-pressure metamorphism (11–13 kbar and 500–540 °C) with a temperature peak of 600 °C in the Tapo Ultramafic Massif, and a greenschist-facies overprint at 2.4–2.6 kbar and 300–330 °C in the enclosing Marañón Complex (Fig. 2). Metamorphic peak conditions were also reported on orthogneiss (12 kbar and 700 °C) and migmatitic paragneiss and garnet-biotite schist (10 kbar and 600 °C) from the Northern and Central parts of the Marañón Complex, respectively (Chew et al., 2005, 2007) (Fig. 2). Cardona et al. (2007, 2009) estimated a similar retrograde metamorphic pathway in mica schists of the Marañón Complex: amphibolite-facies metamorphism (7–10 kbar and 540–660 °C) with greenschist-facies metamorphism overprint at 3–5 kbar and 350–450 °C (Fig. 2).

The investigated chromite-bearing samples come from five chromitite bodies and three serpentinites from the Tapo Ultramafic Massif. The size and dimensions of old quarries left after extraction of the chromitite bodies indicate that these were podiform-like bodies of small size (rarely more than 100 m long and less than 1 m thick), which were enclosed in metaharzburgites, usually in contact with metagabbros (Fig. 1) (Castroviejo et al., 2009; Tassinari et al., 2011).

3. Analytical procedures

The microstructure and zoning of metamorphic chromite grains were imaged using a scanning electron microscope (JEOL SM 6400 SEM) belonging to University of Zaragoza (Spain).

Major and minor elements in chromite and associated silicates were determined using a CAMECA SX-50 at the Serveis Científics i Técnics de la Universitat de Barcelona (Spain), under the following conditions: 15 kV acceleration voltage, 20 nA beam current and 3 μm beam size. Peak counting times were 20 s for Mg, Al, Si, Ti and Cr and 30 s for V, Mn, Fe, Ni and Zn. The calibration for chromite and silicate analysis was performed using natural and synthetic standards: periclase for MgO, corundum for Al_2O_3, diopside for SiO_2, rutile for TiO_2, metallic V, chromite for Cr_2O_3, rhodonite for MnO, Fe_2O_3 for FeO, NiO for NiO, sphalerite for ZnO; the X-ray lines used were the Kα for all the elements. Structural formulae of chromite were calculated assuming stoichiometry following the procedure of Droop (1987).

Thermodynamic modelling was performed using Perple_X software (Connolly, 2009) and the internally consistent thermodynamic database extended to include Cr-bearing phases (cr_hp02ver.dat; Holland and Powell, 1998, revised in 2002). The components considered in the closed system were Cr_2O_3-MgO-FeO-Al_2O_3-SiO_2-H_2O (CrMFASH) and the solid solutions used during calculations were Cr-spinel (Klemme et al., 2009), eskolaite (Chatterjee et al., 1982), olivine, chlorite, orthopyroxene and talc (Holland and Powell, 1998). All other minerals involved in the calculations are pure phases. The Cr-spinel solid solution includes the mixing properties between Cr and Al in the octahedral site based on the subregular solution model of Oka et al. (1984), and between Mg and Fe^{2+} in the tetrahedral site according to the ideal solution model proposed by Engi (1983). Cr-bearing chlorite was not considered because of the lack of experimental data on the mixing parameters for Al and Cr in this mineral.

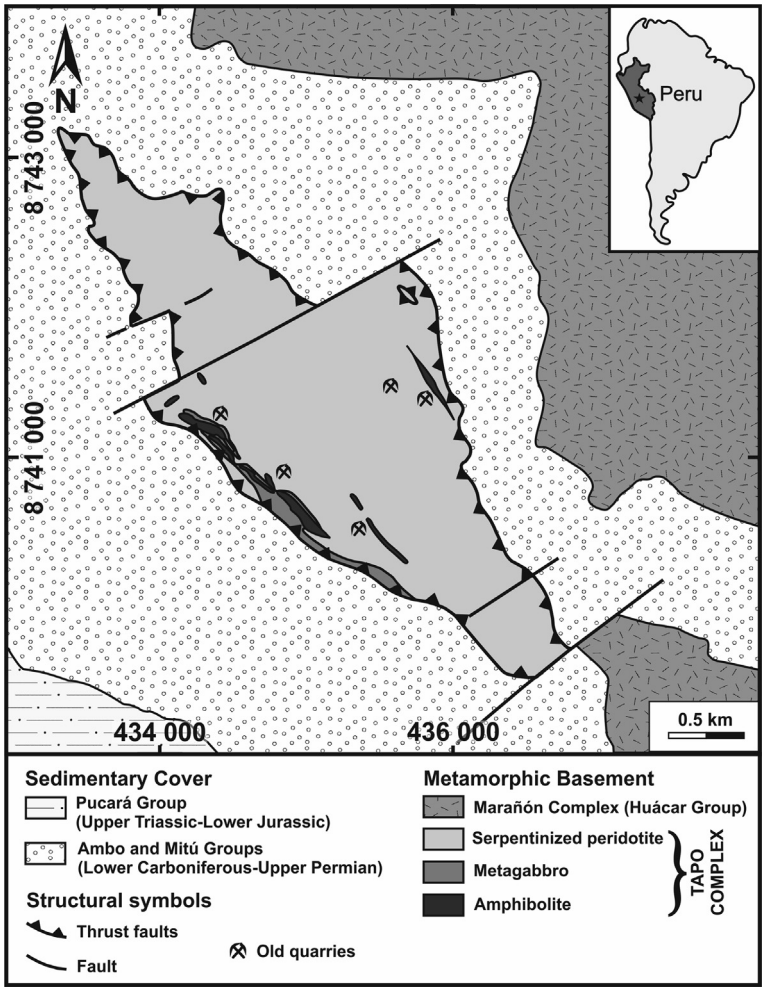

Fig. 1. Simplified geological map of the Tapo Ultramafic Massif hosting the chromitite bodies investigated in this work (modified from Tassinari et al., 2011).

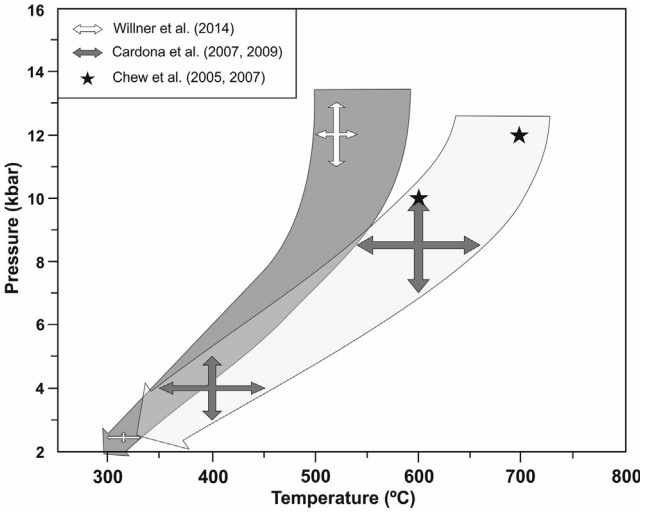

Fig. 2. Pressure-temperature metamorphic pathways calculated at Tapo Ultramafic Massif (Willner et al., 2014) compared with other rocks of Marañón Complex (Cardona et al., 2007, 2009; Chew et al., 2007, 2005). Legend provided as inset in the figure.

4. Petrography and chemistry of the metamorphic chromite

The samples used in this study show variable chromite/silicate ratios, corresponding to semi-massive (60–80 vol% chromite) chromitites and accessory chromite grains (<10 vol% chromite) hosted in serpentinites. Chromite grains may show the three different microstructures of alteration defined by Gervilla et al. (2012). In semi-massive chromitites i) *partly altered chromite* grains are found with relatively homogeneous cores surrounded by porous rims (Fig. 3a) containing chlorite inclusions. However, serpentinites host both ii) *zoned chromite* grains with homogeneous cores irregularly surrounded by non-porous chromite and an outermost rim of magnetite, with antigorite and chlorite inclusions (Fig. 3b); and iii) *non-porous chromite* with mosaic-like texture hosting some inclusions of antigorite (Fig. 3c).

Chlorite is the main silicate between chromite grains in the chromitite samples, while antigorite and irregular patches of magnetite are exclusively found in serpentinites (Fig. 3). No primary olivine was observed in chromitites or in serpentinite samples. Small masses of Ni-rich sulphides and arsenides (heazlewoodite, godlevskite, pentlandite and maucherite) are scattered in the silicate matrix and included in the magnetite patches, pores of partly altered chromite and non-porous rims of zoned chromite grains (Fig. 3a and d).

The microstructural zoning observed in chromite grains correlates directly with variations in their composition. Partly altered chromite grains exhibit an overall trend of decreasing in Al_2O_3 and MgO, coeval with an increase of Cr_2O_3, FeO and to a lesser extent, Fe_2O_3 from core to porous rim (Cr# [Cr/(Cr + Al) in atomic ratio] = 0.41–0.52, Mg# [Mg/(Mg + Fe^{2+}) in atomic ratio] = 0.60–0.79 and $Fe^{3+}/(Fe^{3+} + Fe^{2+}) < 0.33$ in core; Cr# = 0.57–0.95,

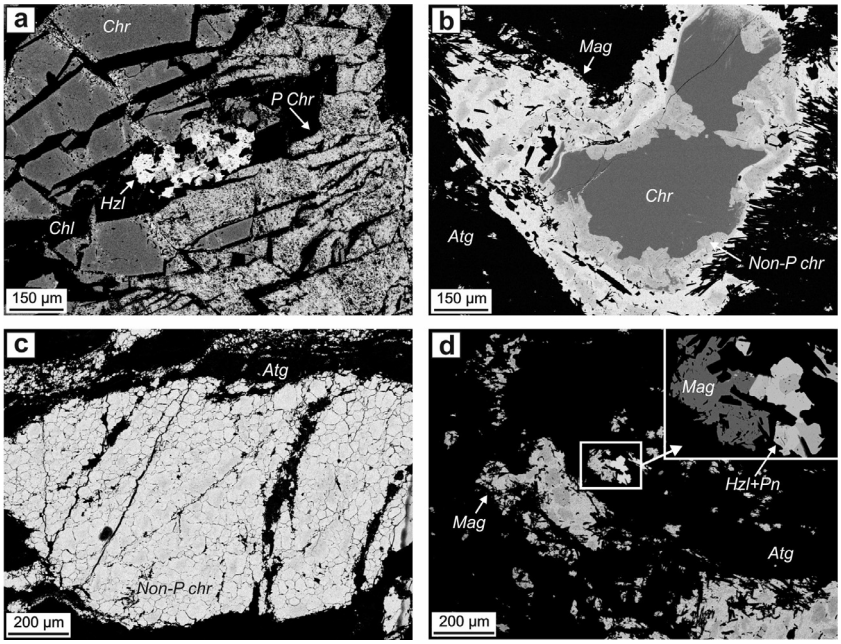

Fig. 3. Back Scattered Electron (BSE) images of the different microstructures of alteration in chromite grains from the Tapo Ultramafic Massif. Partly altered chromite (a) in semi-massive chromitites; zoned (b) and non-porous chromite (c and d) hosted in serpentinites. Abbreviations: Atg: antigorite, Chr: chromite, Hzl: heazlewoodite, Mag: magnetite, Non-P: non-porous chromite, P Chr: porous chromite, Pn: pentlandite. Mineral abbreviations after Whitney and Evans (2010).

Mg# = 0.19–0.69 and $Fe^{3+}/(Fe^{3+} + Fe^{2+}) < 0.62$ in porous rim) (Fig. 4a–c and Table 1). This trend is more evident, especially for Fe_2O_3, from core (Cr# = 0.50–0.55, Mg# = 0.43–0.66 and $Fe^{3+}/(Fe^{3+} + Fe^{2+}) = 0.16–0.25$) to non-porous and magnetite rims of zoned chromite grains (Cr# = 0.67–0.99, Mg# = 0.05–0.33 and $Fe^{3+}/(Fe^{3+} + Fe^{2+}) = 0.37–0.60$ in non-porous rim; Cr# = 0.95–1.00, Mg# = 0.01–0.11 and $Fe^{3+}/(Fe^{3+} + Fe^{2+}) = 0.63–0.67$ in magnetite rim) (Fig. 4d–f and Table 1). The composition of non-porous chromite overlaps that of magnetite rims of zoned chromite grains (Cr# = 0.98–1.00, Mg# < 0.09 and $Fe^{3+}/(Fe^{3+} + Fe^{2+}) = 0.51–0.67$) (Fig. 4d–f and Table 1).

The average composition of chlorite associated with partly altered chromite in semi-massive chromitites is $(Mg_{4.41}Al_{1.31}Cr_{0.14}Fe_{0.12}Ni_{0.03})_{\Sigma=6.00}(Si_{2.63}Al_{1.37})_4O_{10}(OH)_8$, and that related with zoned chromite in serpentinites is $(Mg_{4.92}Al_{0.73}Fe_{0.25}Cr_{0.05}Ni_{0.02})_{\Sigma=5.97}(Si_{3.25}Al_{0.75})_4O_{10}(OH)_8$ (Table 2). Both contain significant amounts of Cr_2O_3 (1.22–9.53 wt% in semi-massive chromitites and 0.29–1.48 wt% in serpentinites). Composition of antigorite associated with zoned and non-porous chromite in serpentinites is $(Mg_{2.73}Fe_{0.11}Al_{0.07}Ni_{0.01}Cr_{0.01})_{\Sigma=2.93}Si_{2.01}O_5(OH)_4$ (Table 2).

4.1. Estimations on the chromitite bulk composition

In order to know the compositional differences between unaltered and altered chromitite bodies their bulk composition was calculated from unaltered semi-massive chromitite and considering a 72:28 molar mix of primary chromite and olivine (Table 3). These molar proportions were estimated from the areal proportion of chromite and silicate matrix on a thin section image of a semi-massive chromitite sample from the Tapo Ultramafic Massif, using the Image-J software (Rasband, 2007) and assuming that olivine was the only primary silicate mineral in the matrix. The composition of primary chromite is that of the average values of the cores of partly altered chromite grains from the studied thin section $[(Mg_{0.74}Fe_{0.26})Cr_{0.98}Al_{1.02}O_4]$ and that of olivine is Fo_{92} $[(Mg_{1.84}Fe_{0.16})SiO_4]$, the typical olivine composition in mantle-hosted ophiolitic chromitites (Dick and Bullen, 1984; Leblanc and Nicolas, 1992; Kamenetsky and Gurenko, 2007; Tian et al., 2011) (Table 3).

The estimated bulk composition of unaltered semi-massive chromitites is 15.48 mol% Cr_2O_3, 45.96 mol% MgO, 10.18 mol% FeO, 16.10 mol% Al_2O_3 and 12.28 mol% SiO_2 (Table 3).

Altered semi-massive chromitite bulk composition was calculated by assuming a 40:60 molar mix of altered chromite and clinochlore (Table 3). Proportions of altered chromite and chlorite were calculated after the following equation:

$$V_{alt} = (V_{unalt} - 48.001)/0.5886 \quad (1)$$

where V_{alt} (vol%) is the modal volume of chromite in altered chromitites and V_{unalt} (vol%) is that in unaltered chromitites. Eq. (1) is deduced from the calibration line obtained by plotting the volume of altered chromite calculated from pseudosections computed for 90:10, 80:20, 70:30, and 60:40 molar mixes of primary chromite and olivine (Fig. 5). V_{alt} is the minimum volume selected at the lowest temperature conditions (c.a. 250 °C) or prior to the stability of diaspore (Appendix 1), and represents the complete re-equilibration between chromite and olivine under hydrous conditions (i.e., complete alteration of unaltered chromitite). The composition of altered chromite is the average of the porous rim in partly altered chromite from the studied thin section $[(Mg_{0.62}Fe_{0.38})Cr_{1.2}Al_{0.8}O_4]$ (Table 3), and that of chlorite is clinochlore $[Mg_5AlSi_3Al(OH)_8]$ because the content of FeO in chlorite in equilibrium with partly altered chromite is very low (ca. 1.47 wt%; Table 2). Compared to the unaltered semi-masive chromitite, the altered semi-massive chromitite has lower MgO (35.97 mol%), higher SiO_2 (16.86 mol%) but similar contents of Cr_2O_3 (18.44 mol%), FeO (12.21 mol%) and Al_2O_3 (16.52 mol%) (Table 3).

5. Discussion

5.1. Chromite-matrix silicate reactions form metamorphic zoning in chromite

The different microstructures and zoning patterns exhibited by chromite grains from the Tapo Ultramafic Massif are similar to those described in other chromite grains affected by retrograde hydrous metamorphism (Gervilla et al., 2012; Prabhakar and

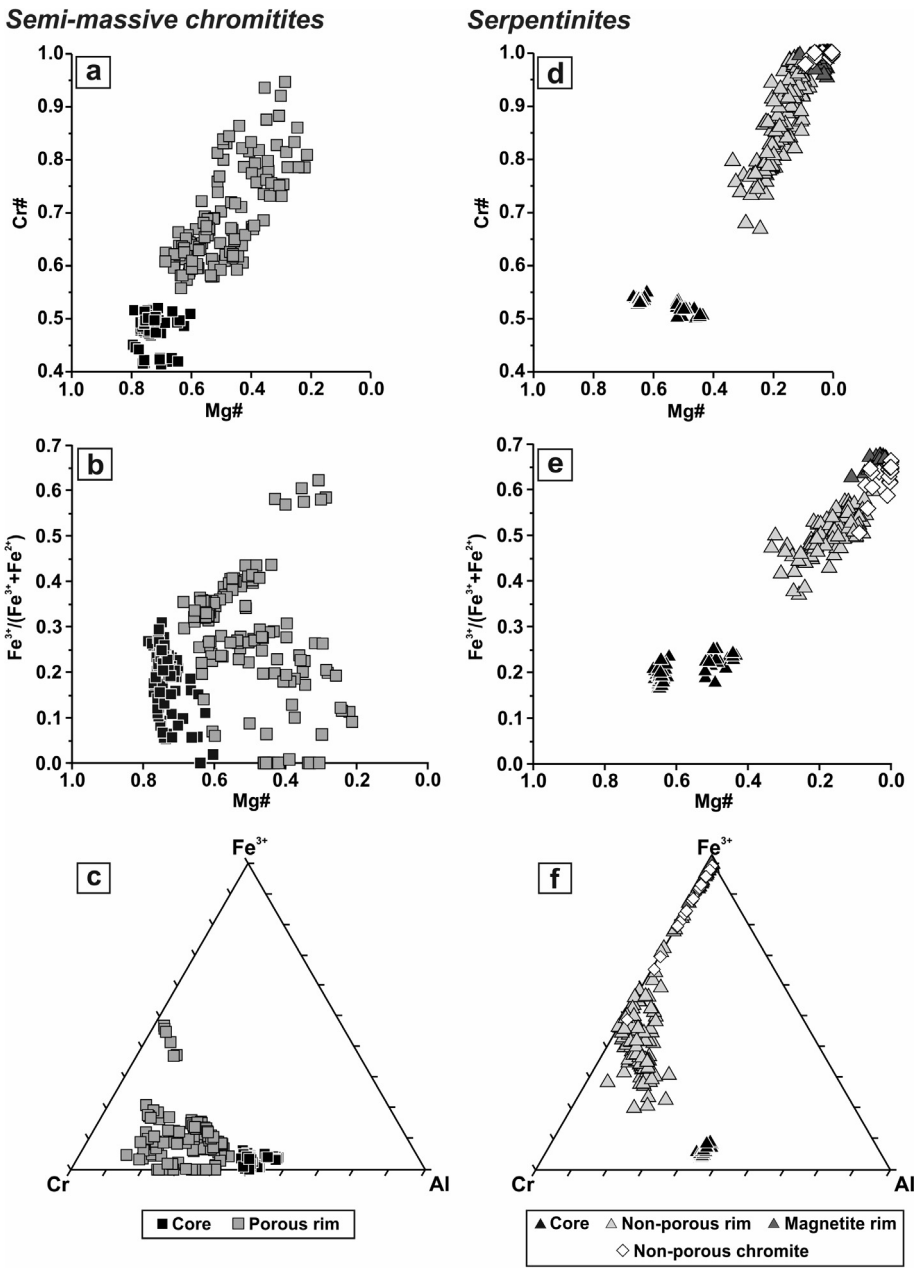

Fig. 4. Compositional variations of chromite from the studied semi-massive chromitites (a-c) and serpentinites (d-f) in terms of Mg# [Mg/(Mg + Fe^{2+}) atomic ratio] versus Cr# [Cr/(Cr + Al) atomic ratio] and $Fe^{3+}/(Fe^{3+} + Fe^{2+})$ (atomic ratio), and the ternary Cr-Fe^{3+}-Al diagram. Legend provided as inset in the figure.

Bhattacharya, 2013; Barra et al., 2014; Colás et al., 2014; Satsukawa et al., 2015; Ahmed and Surour, 2016). These microstructures and zoning can be explained as a consequence of the two stage process suggested by Gervilla et al. (2012). The first stage involved the reaction between primary chromite and olivine in presence of SiO_2-rich fluids to produce a core-to-rim trend of Al_2O_3 and MgO loss and Cr_2O_3 and FeO gain (Figs. 3a and 4a–c) in chromite grains. These compositional trends reflect the preferential partitioning of Al and Mg towards chlorite that crystallized coeval with Fe^{2+}-rich porous chromite (e.g., Gervilla et al., 2012; Colás et al., 2014) (Fig. 6). The balanced equation of this reaction can be written as follows (Fig. 6):

$$2(Mg_{0.74}Fe_{0.26})CrAlO_4 + 2(Mg_{1.84}Fe_{0.16})SiO_4 + SiO_{2aq.} + 8H_2O \rightarrow (Mg_{4.51}Fe_{0.49})AlSi_3Al(OH)_8 + (Mg_{0.65}Fe_{0.35})Cr_2O_4$$

$$\text{Chromite} + \text{Olivine} \rightarrow \text{Clinochlore} + Fe^{2+}\text{-rich chromite} \quad (2)$$

The second stage of alteration is the result of the exhaustion of olivine and the subsequent increase of fO_2 in the fluid, which promoted the oxidation of Fe^{2+} and the increase of Fe^{3+} in the system (Colás et al., 2014 and references therein). The interaction of previous Fe^{2+}-rich porous chromite with these more oxidizing and Fe-bearing fluids, resulted in a more pronounced loss of Al_2O_3 and MgO coeval with an extreme increase of Fe_2O_3 and to lesser extent for Cr_2O_3 and FeO (Figs. 3b–d and 4d–e). These trends, that can be observed from core to non-porous rims in zoned and non-porous chromite grains, indicate the diffusion of Fe^{2+} and Fe^{3+} through the pore network while eliminating the porous textures and producing Fe^{3+}-rich non-porous chromite (i.e., ferrian chromite) (Mukherjee et al., 2010; Gervilla et al., 2012; Colás et al., 2014; Satsukawa et al., 2015) (Fig. 6). A balanced equation of this second reaction is:

$$(Mg_{0.65}Fe_{0.35})Cr_2O_4 + Fe_3O_{4aq} \rightarrow 2(Fe_{0.68}Mg_{0.32})CrFeO_4$$

$$Fe^{2+}\text{-rich chromite} + \text{Magnetite} \rightarrow \text{Ferrian chromite} \quad (3)$$

Table 1
Average composition of altered chromite grains from the Tapo Ultramafic Massif (Peru) analyzed by EMPA.

Texture	Semi-massive chromitite		Accessory chromite in sepentinite			
Chromite microstructure	Partly altered chromite		Zoned chromite			Non-porous chromite
Chromite grain zone	Core	Porous rim	Core	Non-porous rim	Magnetite rim	Core to rim
	n = 107	n = 134	n = 72	n = 137	n = 41	n = 27
TiO_2 (wt%)[a]	0.15 ± 0.03	0.20 ± 0.07	0.14 ± 0.02	0.33 ± 0.54	0.10 ± 0.11	0.11 ± 0.18
Al_2O_3	28.16 ± 1.86	16.73 ± 5.08	24.79 ± 0.36	3.47 ± 2.94	0.00 ± 0.04	0 ± 0.10
Cr_2O_3	40.51 ± 1.84	45.74 ± 4.77	42.45 ± 1.83	34.82 ± 4.07	1.68 ± 4.47	5.83 ± 6.84
Fe_2O_3[b]	3.19 ± 1.09	7.68 ± 6.37	3.85 ± 1.27	29.78 ± 5.93	67.53 ± 4.78	62.25 ± 7.84
FeO	10.40 ± 1.22	17.39 ± 3.04	14.12 ± 2.65	25.28 ± 1.50	30.03 ± 0.91	30.91 ± 0.52
V_2O_3	0.15 ± 0.04	0.17 ± 0.04	0.16 ± 0.04	0.11 ± 0.04	0.04 ± 0.03	0.05 ± 0.03
MnO	0.22 ± 0.10	0.76 ± 0.73	0.25 ± 0.09	2.06 ± 0.45	0.13 ± 0.32	0.08 ± 0.16
MgO	16.88 ± 0.90	10.66 ± 2.84	14.11 ± 1.77	2.895 ± 1.42	0.51 ± 0.33	0.06 ± 0.49
ZnO	0.06 ± 0.06	0.14 ± 0.54	0.15 ± 0.13	0.545 ± 0.17	0.02 ± 0.06	0.06 ± 0.20
NiO	0.22 ± 0.05	0.08 ± 0.12	0.14 ± 0.04	0.28 ± 0.10	0.51 ± 0.06	0.27 ± 0.06
Total	100.2 ± 0.8	100.3 ± 0.9	100.4 ± 0.6	99.8 ± 0.8	100.5 ± 0.9	99.7 ± 0.7
Atoms per formula unit calculated on the basis of 4 oxygens						
Al	0.97	0.63	0.88	0.15	0.00	0.00
Cr	0.94	1.16	1.01	1.00	0.05	0.18
Fe^{3+}	0.07	0.19	0.09	0.82	1.94	1.81
V	0.00	0.00	0.00	0.00	0.00	0.00
Mg	0.74	0.51	0.64	0.16	0.03	0.00
Fe^{2+}	0.26	0.47	0.36	0.77	0.96	1.00
Ti	0.00	0.00	0.00	0.01	0.00	0.00
Mn	0.01	0.02	0.01	0.06	0.00	0.00
Ni	0.01	0.00	0.00	0.01	0.02	0.01
Cr#[c]	0.41–0.52	0.57–0.95	0.50–0.55	0.67–0.99	0.95–1.00	0.98–1.00
Mg#[d]	0.60–0.79	0.19–0.69	0.43–0.66	0.05–0.33	0.01–0.11	<0.09
$Fe^{3+}/(Fe^{3+}+Fe^{2+})$[e]	0.00–0.33	0.00–0.62	0.16–0.25	0.37–0.60	0.63–0.67	0.51–0.67

[a] Uncertainties are given as 1σ standard deviation.
[b] Fe_2O_3 contents of chromite were computed assuming R_3O_4 stoichiometry and charge balance.
[c] Range of Cr# [Cr/(Cr + Al) atomic ratio].
[d] Range of Mg# [Mg/(Mg + Fe^{2+}) atomic ratio].
[e] Range of $Fe^{3+}/(Fe^{3+} + Fe^{2+})$ in atomic ratio.

Table 2
Average composition of silicates from the Tapo Ultramafic Massif (Peru) analyzed by EMPA.

Rock type	Semi-massive chromitite		Sepentinite			
Mineral	Chlorite n = 36		Chlorite n = 6		Antigorite n = 32	
SiO_2 (wt%)[a]	28.15	±2.3	34.74	±0.52	44.07	±0.95
Al_2O_3	24.32	±5.01	13.61	±0.93	1.38	±0.49
Cr_2O_3	1.85	±1.88	0.71	±0.46	0.15	±0.24
FeO	1.47	±0.48	3.16	±0.24	2.84	±4.02
MgO	31.61	±1.25	35.46	±0.37	40.05	±1.80
NiO	0.19	±0.36	0.125	±0.03	0.1	±0.08
Total	87.6	±0.8	87.81	±0.9	88.61	±1.9
Atoms per formula unit[b]						
Si^{IV}	2.63		3.25		2.01	
Al^{IV}	1.37		0.75			
Al^{VI}	1.31		0.73		0.07	
Cr	0.14		0.05		0.01	
Mg	4.41		4.92		2.73	
Fe^{2+}	0.11		0.25		0.11	
Ni	0.03		0.02		0.01	

[a] Uncertainties are given as 1σ standard deviation.
[b] Atoms per formula unit calculated on the basis of 14 oxygens for chlorite and on the basis of 9 oxygens for antigorite.

The formation of magnetite rims in zoned chromite grains and magnetite patches hosted in the silicate matrix (Figs. 3b and d and 6) evidences the excess of Fe in the system once the reaction of formation of ferrian chromite has been completed. This may reflect a continuous supply of Fe-bearing fluids from country rocks which were coevally being serpentinized. However, the preservation of partly altered chromite in semi-massive chromitites suggests an unequal effectiveness of the process, which is highly affected by the chromite/silicate and fluid/rock ratios, higher and lower respectively in semi-massive chromitites relative to serpentinites (Loferski, 1986; Candia and Gaspar, 1997; Proenza et al., 1999; Merlini et al., 2009; Barra et al., 2014; Colás et al., 2014).

Table 3
Bulk composition of altered and unaltered semi-massive chromitites obtained from the Tapo Ultramafic Massif (Peru). Average composition of chromite was analyzed by EMPA.

	Unaltered chromitite		Altered chromitite	
	Chromite cores	Olivine[a]	Porous chromite	Clinochlore[b]
	n = 51		n = 22	
SiO_2 (wt%)[c]	0.04 ± 0.04	41.47	0.03 ± 0.12	32.28
TiO_2	0.16 ± 0.02		0.20 ± 0.07	
Al_2O_3	27.79 ± 0.66		20.23 ± 1.67	18.11
Cr_2O_3	40.36 ± 0.56		45.47 ± 1.30	
Fe_2O_3[d]	3.51 ± 0.55		5.71 ± 1.93	
FeO	10.44 ± 0.56	7.85	14.24 ± 1.27	
V_2O_3	0.14 ± 0.05		0.16 ± 0.03	
MnO	0.23 ± 0.09		0.51 ± 0.25	
MgO	16.67 ± 0.35	50.68	13.10 ± 0.94	35.82
ZnO	0.07 ± 0.04		0.11 ± 0.05	
NiO	0.22 ± 0.05		0.08 ± 0.05	
Total	99.63 ± 0.62	100.0	99.83 ± 0.83	86.21
Atoms per formula unit				
SiO_2	0.00	2.01	0.00	3.01
Al^{IV}				0.99
Al^{VI}	0.97		0.74	1.01
Cr	0.94		1.12	0.00
Fe^{3+}	0.08		0.13	
V	0.00		0.00	
Mg	0.73	1.83	0.61	4.98
Fe^{2+}	0.26	0.16	0.37	0.00
Ti	0.00		0.00	
Mn	0.01		0.01	
Ni	0.00		0.00	
Cr#[e]	0.49		0.60	
Mg#[f]	0.74	92.00	0.62	
$Fe^{3+}/(Fe^{3+} + Fe^{2+})$[g]	0.23		0.26	
	72:28 Chromite:Olivine		40:60 Chromite:Chlorite	
SiO_2 (mol%)	12.28		16.86	
Al_2O_3	16.10		16.52	
Cr_2O_3	15.48		18.44	
FeO	10.18		12.21	
MgO	45.96		35.97	

[a] Average composition of stoichiometric Fo_{92}.
[b] Average composition of stoichiometric clinochore.
[c] Uncertainties are given as 1σ standard deviation.
[d] Fe_2O_3 contents of chromite were computed assuming R_3O_4 stoichiometry and charge balance.
[e] Range of $Cr^{\#}$ [Cr/(Cr + Al) atomic ratio].
[f] Range of $Mg^{\#}$ [Mg/(Mg + Fe^{2+}) atomic ratio].
[g] Range of $Fe^{3+}/(Fe^{3+} + Fe^{2+})$ in atomic ratio.

5.2. Thermodynamic basis for accounting the effect of silica and magnesium during alteration of chromite

Previous thermodynamic approaches applied to model the alteration of chromite during metamorphism considered it as a solid-stage diffusion process (Gervilla et al., 2012; Barra et al., 2014; González-Jiménez et al., 2015, 2016). In these models the effects of metamorphic alteration on the igneous textures, mineral assemblages and bulk composition of the rocks and minerals were estimated using binary pressure-temperature (P-T) pseudosections. The application of this modelling to chromitites from the Tapo Ultramafic Massif predicts the existence of brucite-bearing assemblages at low P-T conditions (i.e., greenschist-facies metamorphism; Appendix 1). However, we observed chlorite instead of brucite in our samples (Fig. 3a) as well as lower MgO and higher SiO_2 contents in the bulk-rock of altered chromitite relative to unaltered chromitite (Table 3). These observations suggest the possible addition of SiO_2 and the possible leaching of MgO by metamorphic fluids in an open system. The irregular contact between cores and Fe^{2+}-rich porous rims in partly altered chromite and the presence of chlorite filling these pores led us to suggest a mechanism of alteration of chromite dominated by dissolution-precipitation rather than solid-state diffusion driven process, similarly to observed in the metamorphosed chromitites of the Golyamo-Kamenyane serpentinites by Gervilla et al. (2012) and Colás et al. (2014). This process that is predominantly identified along the interface chromite grain edge-fluid can be better modeled applying a hybrid chemical potential-bulk composition approach (i.e., T-μ and μ-μ pseudosections), such as recently suggested Evans et al. (2013) in the case of serpentinites from New Caledonia.

Figs. 7a and b show T-μSiO_2 and T-μMgO pseudosections performed for chromitites from the Tapo Ultramafic Massif and calculated considering a water-saturated CrMFASH system, for an unaltered semi-massive chromitite bulk composition (72:28 molar mix of primary chromite and olivine; Section 4.1.) at a constant pressure of 2 kbar. This pressure was chosen because it is consistent with the formation conditions of chlorite (see Eq. (2); Fig. 6) and is slightly below the lowest metamorphic pressure conditions obtained by Willner et al. (2014) in metabasites and metapelites from the Tapo Ultramafic Massif (2.4 kbar) and by Chew et al. (2005, 2007) and Cardona et al. (2007, 2009) in migmatites and metapelites from the Marañón Complex (3 kbar; Fig. 2).

As is shown in Figs. 7a and b, the tetravariant field consisting of the assemblage olivine + chromite (dark grey field in Fig. 7a and b) is stable at temperatures above 520 °C and variable μSiO_2 (e.g., below −910 kJ/mol) and μMgO (e.g., between −562 and −594 kJ/mol). This field represents the stable assemblage of an unaltered

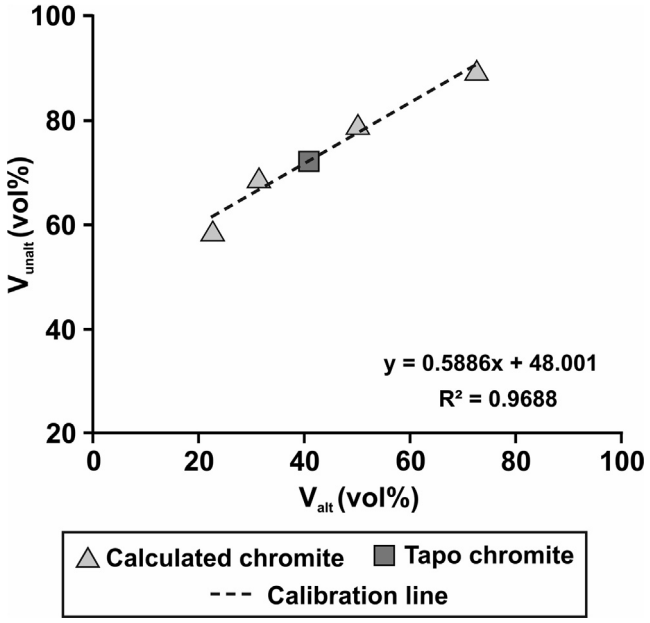

Fig. 5. Plot of the modal volume variations of chromite from altered chromitites (V_{alt}) versus that of unaltered chromitites (V_{unalt}) computed for 90:10, 80:20, 70:30 and 60:40 molar mixes of primary chromite and olivine.

semi-massive chromitite (Fig. 6). However, at temperatures of 300 °C (i.e., lowest temperature conditions inferred from the host ultramafic rocks in the Tapo Ultramafic Massif and from the Marañón Complex; Willner et al., 2014; Chew et al., 2005, 2007; Cardona et al., 2007, 2009) chlorite is predicted to be stable with chromite instead of brucite (i.e., assemblage chlorite + chromite; dark grey field in Fig. 7a and b) at higher μSiO_2 (e.g., from −915 to −876 kJ/mol) but lower μMgO (e.g., from −598 to −579 kJ/mol) conditions. This field should represent the stable assemblage for altered chromitites (i.e., Fe^{2+}-rich chromite and chlorite) showed in semi-massive chromitites the Tapo Ultramafic Massif. Thus, these diagrams predict the metamorphic reaction explaining the formation of partly altered chromite (see Eq. (2)). If so, Figs. 7a and b reproduce the mineral assemblages in semi-massive chromitites (Fig. 3a) before and after alteration due to changing μSiO_2 and μMgO conditions. This suggests that variation in SiO_2 and MgO most likely due to an influx of external fluids carrying these components in solution. Therefore, the thermodynamic calculations used to explain the alteration of chromitite bodies and their forming chromite grains must be performed in an open system relative to SiO_2 and MgO.

A μSiO_2-μMgO diagram (Fig. 7c) was performed in order to investigate the effects of simultaneous changes in SiO_2 and MgO during alteration of chromite. Fig. 7c shows a pseudosection calculated for a water-saturated unaltered semi-massive chromitite, with a bulk composition corresponding to a 72:28 molar mix of primary chromite and olivine (Table 3), at constant P-T conditions of 2 kbar and 300 °C. This diagram reproduces with fidelity the phase relations changes observed from unaltered to altered semi-massive chromitites (see dashed line in Fig. 7c). Primary chromite is stable at low μSiO_2 but high μMgO (dark grey field in Fig. 7c), while the chromite + chlorite and chromite + chlorite + eskolaite assemblages (i.e., Fe^{2+}-porous rims in partly altered chromite) are stable at progressive higher μSiO_2 but lower μMgO (grey and white fields in Fig. 7c). Eskolaite (Cr_2O_3) is stable in this field but it is not present in the studied samples. However, at the mentioned P-T conditions the amount of this mineral reaches 7.20 wt%, which is similar to the content of Cr_2O_3 observed in chlorite from partly altered chromite (up to 9.53 wt% Cr_2O_3). Due to the lack of a Cr-rich end-member in the chlorite solution model, the estimated content of eskolaite could represent the high Cr_2O_3 amounts analyzed in the chlorite associated with partly altered chromite from semi-massive chromitites at the Tapo Ultramafic Massif. Therefore, the divariant field Chl + Chr + Esk modeled in Fig. 7c is closer to the assemblage described in altered semi-massive chromitites (Fig. 3a) than the trivariant field Chl + Chr obtained for unaltered semi-massive chromitite (grey field in Fig. 7c). The good agreement between observed and modeled mineral assemblages in altered semi-massive chromitite from the Tapo Ultramafic Massif supports the important role of SiO_2 and MgO in the retrograde metamorphic evolution of chromitite bodies.

5.3. The role of SiO_2 and MgO in the alteration of the Tapo Ultramafic Massif chromitites

Chemical potential diagrams provided in Fig. 7 show the possible phase relations that might result during the alteration of

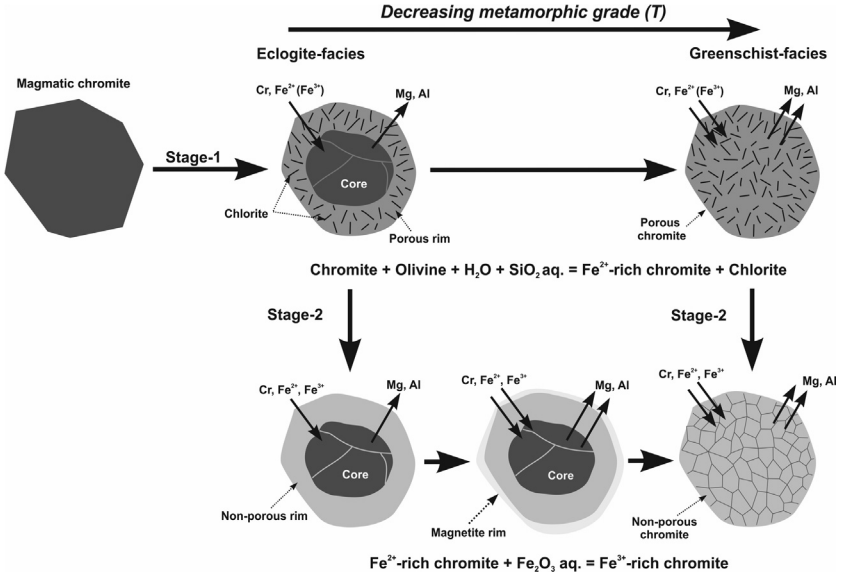

Fig. 6. Schematic illustration of microstructural and compositional changes in chromite grains, showed as a two-stage process of alteration during the retrograde metamorphic evolution of the Tapo Ultramafic Massif. The extent of reaction is noted in the figure with the number of arrows.

semi-massive chromitites from the Tapo Ultramafic Massif at 2 kbar and 300 °C (i.e., latest overprint inferred from the Tapo Ultramafic Massif and Marañón Complex) and increasing μSiO_2 but decreasing μMgO. However, these diagrams cannot include altogether the unaltered and altered chromitite bulk compositions, μSiO_2 and μMgO as thermodynamic variables and the different P-T pathways estimated for the enclosing metamorphic rocks. The careful application of P-T-X diagrams becomes an appropriate tool as they take the latter parameters into account and allow the observed phase relation changes to be monitored during the chromite alteration process.

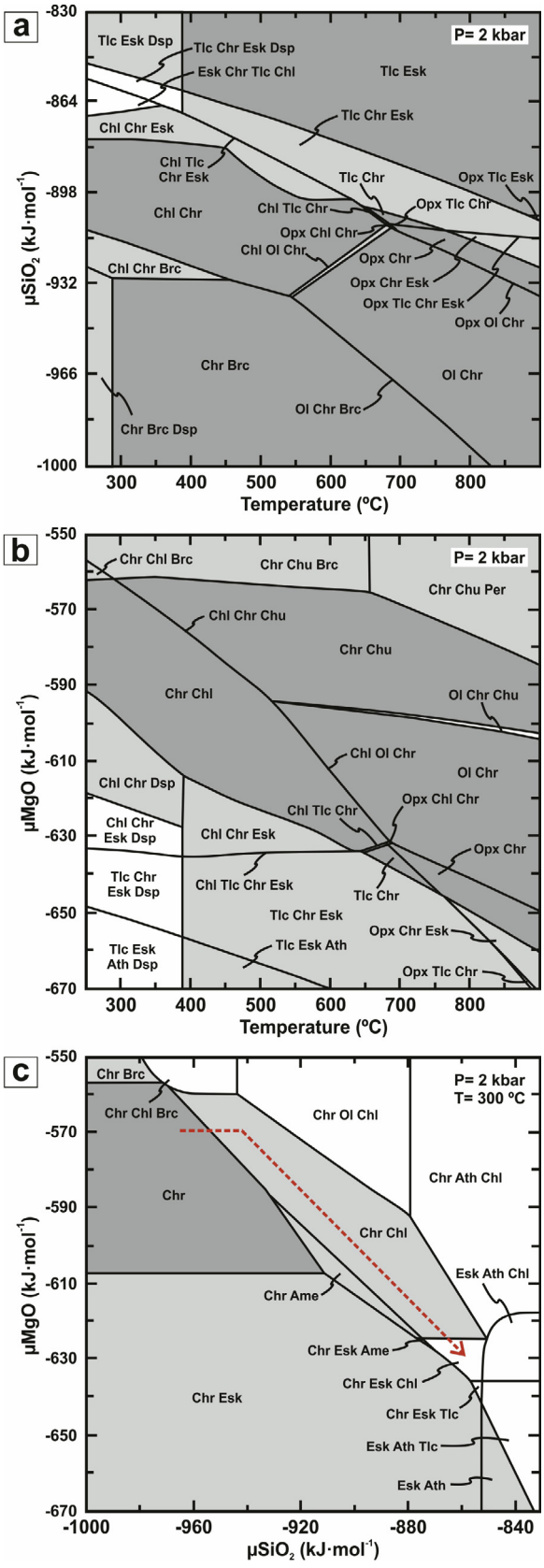

Fig. 8 shows P-T-X diagrams (fluid saturated CrMFASH system and contoured for SiO_2 wt% and MgO wt%) calculated using the different P-T paths estimated for the retrograde metamorphism that affected the metamorphic basement enclosing the Tapo Ultramafic Massif (i.e., Marañón Complex) and the rocks of the massif itself. The diagrams shown in this figure correspond to metamorphic pathways recorded in the metabasitic and metapelitic rocks of the Tapo Ultramafic Massif (T = 0.03P + 505 from 16 to 2.4 kbar and from 685 to 300 °C; Willner et al., 2014) and the enclosing migmatitic and metapelitic rocks of the Marañón Complex (T = 0.04P + 506 from 12 to 3 kbar and from 700 to 350 °C; Cardona et al., 2007, 2009; Chew et al., 2005, 2007), respectively. The bulk composition variability (X) represents a transition from unaltered (72:28 molar mix of primary chromite and Fo_{92}) (X_{C1}) to altered chromitite bulk compositions (40:60 molar mix of altered chromite and clinochlore) (X_{C2}).

P-T-X diagrams (Fig. 8) show that the olivine + chromite assemblage (i.e., unaltered chromitite) was stable only at high P-T conditions and for X_{C1} values close to 1. Lowering pressure and temperature, following the red arrows in Fig. 8, allowed to produce the observed progressive stabilization of the following assemblages: chlorite + olivine + chromite, chlorite + chromite and chlorite + chromite + eskolaite (i.e., the altered chromitite assemblage) upon increasing the SiO_2 contents (>10.90 wt% SiO_2; Fig. 8a and c) and decreasing that of MgO (<21.00 wt% MgO) (Fig. 8b and d). However, the stabilization of chlorite + chromite + brucite occurs at lower SiO_2 and higher MgO contents (<10.90 wt% SiO_2 and >21.00 wt% MgO; Fig. 8). This means that P-T-X diagrams show the partial equilibrium sequence of mineral assemblages during the retrograde metamorphic evolution of semi-massive chromitites from the Tapo Ultramafic Massif.

Figs. 9 shows that the composition of metamorphic chromite predicted by our thermodynamic model (i.e., following the metamorphic pathways proposed at Tapo Ultramafic Massif and Marañón Complex) perfectly matches with that determined for natural chromite grains from the Tapo Ultramafic Massif. Thus, the composition of predicted chromite follows the observed trend of Al_2O_3 and MgO decrease and Cr_2O_3 and FeO increase from core to porous rim in the partly altered chromite grains from semi-massive chromitites. These observations suggest that the natural chromite we have studied only preserved the record of the metamorphic peak P-T conditions and of the latest overprint (i.e., chromite + olivine and chlorite + chromite + eskolaite assemblages, respectively), but not that corresponding to the complete metamorphic pathway. This is similar to what is observed in zoned chromite grains from Tehuitzingo serpentinite (Mexico, Proenza et al., 2004), Río de Las Tunas belt (Argentina, Gargiulo et al., 2013) or La Cabaña (Chile, González-Jiménez et al., 2016) where

Fig. 7. Temperature (T)-μSiO_2 (a), T-μMgO (b) and μSiO_2-μMgO (c) pseudosections for unaltered semi-massive chromitite (72:28 molar mix of primary chromite and olivine) bulk composition in the fluid saturated CrMFASH system, calculated at constant pressure and temperature. Dashed line reproduces the phase relations changes observed from unaltered to altered semi-massive chromitites. Mineral abbreviations after Whitney and Evans (2010), where amesite is Ames, antigorite is Atg, anthophyllite is Ath, brucite is Brc, chlorite is Chl, chromite is Chr, clinohumite is Chu, diaspore is Dsp, eskolaite is Esk, olivine is Ol, orthopyroxene is Opx, periclase is Per and talc is Tlc.

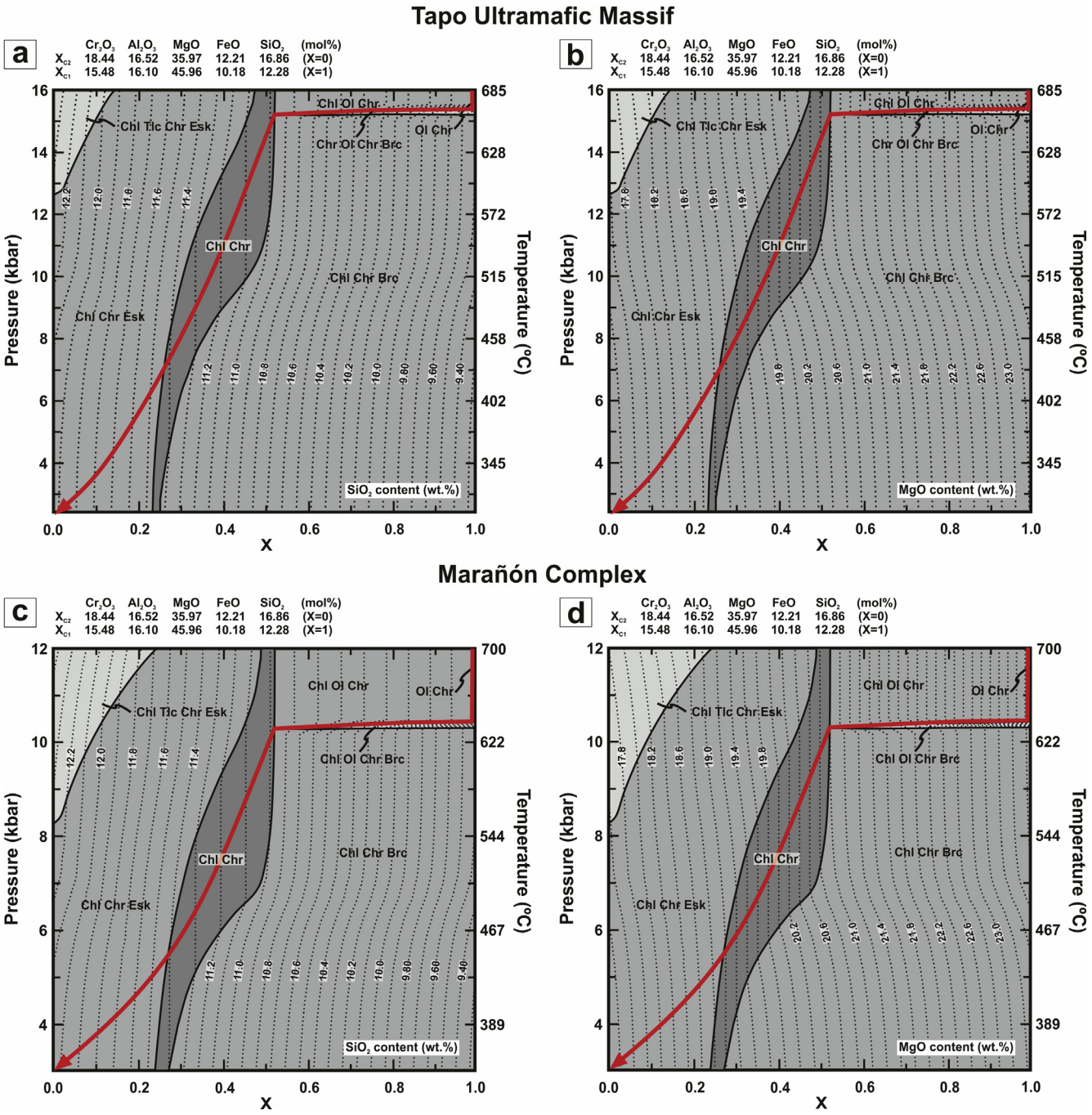

Fig. 8. P-T-X pseudosections calculated for unaltered semi-massive chromitite composition at X_1 and altered semi-massive chromitite composition at X_2 in the water-saturated CrMFASH system. Metamorphic gradients are (a–b) T = 0.03P + 505, for a P = 16–2.4 kbar and T = 685–300 °C, for the Tapo Ultramafic Massif metamorphism; and (c-d) T = 0.04P + 506, for P = 12–3 kbar and T = 700–350 °C, for the Marañón Complex metamorphism. Dashed lines correspond to the content of SiO_2 (a–**c**) and MgO (b–d) (wt%) in the system. The red arrows show the P-T exhumation paths proposed for semi-massive chromitite bodies of the Tapo Ultramafic Massif. Mineral names as in Fig. 7.

metamorphosed chromitites and their metamorphic host rocks only recorded the metamorphic peak and the latest overprint.

5.4. Origin of the SiO_2-rich fluids and mobilization of MgO from the chromitites

Bach et al. (2006) and Frost et al. (2013) suggest that the hydration of orthopyroxene during serpentinization adds SiO_2 to the circulating fluids, which usually react with brucite in presence of olivine to form serpentinite and a residual solution with MgO as an aqueous species (Majumdar et al., 2016). In addition, the hydration of olivine from the peridotite and/or dunite hosting chromitites usually lowers fO_2 (e.g., Bach et al., 2006) and produces reducing fluids that might transform the magmatic chromite to partly altered chromite (see Eq. (2)). Similarly, the alteration of chromite grains in semi-massive chromitite bodies from the Tapo Ultramafic Massif could have taken place due to the circulation of reducing and SiO_2-rich fluids that leached MgO out from the rock.

Experiments performed by Brenan and Rose (2002) in chromite and olivine mix suggest that the presence of silicates, mainly olivine, in chromite-rich rocks reduce the permeability of natural

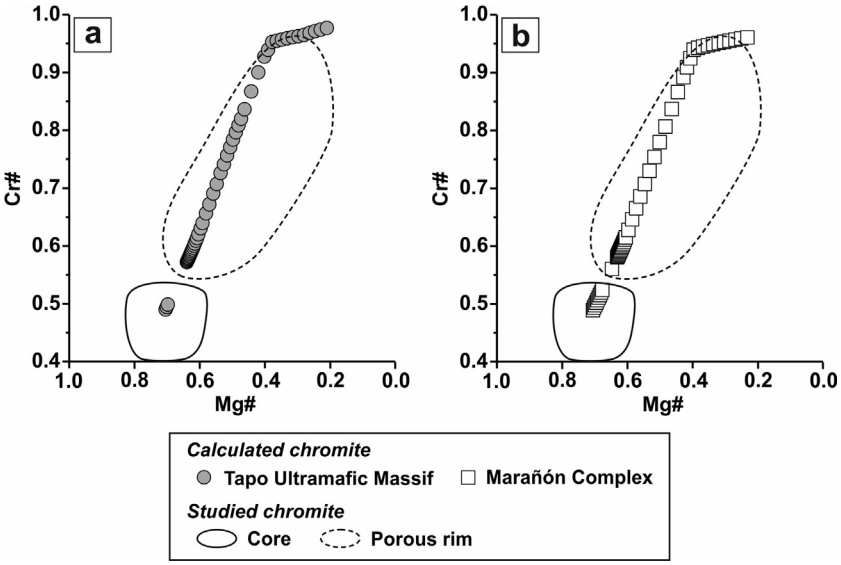

Fig. 9. Compositional variations of chromite in terms of Mg# [Mg/(Mg + Fe^{2+}) atomic ratio] versus Cr# [Cr/(Cr + Al) atomic ratio] calculated from P-T-X pseudosections following the metamorphic pathways proposed at (a) Tapo Ultramafic Massif and (b) Marañón Complex.

chromitites. This is in disagreement with our observations taken from the different microstructures of chromite grains and the results obtained applying the thermodynamic modelling, which clearly suggest that the infiltration of SiO_2-rich fluids and the mobilization of MgO (Figs. 7 and 8) enhanced the transformation of magmatic chromite in chromitites to Fe^{2+}-rich porous chromite (Fig. 3a). Putnis (2002, 2009, 2015) and Putnis and Austrheim (2010) suggested that the dissolution-precipitation processes arising from the hydrous metamorphism generate a transient porosity in the product phase, but it is only effective during the replacement process (i.e., in presence of fluids). The analysis of magmatic and metamorphic chromite grains from ophiolitic chromitites by Gervilla et al. (2012) and Lenaz et al. (2007) indicate that the cell size of primary chromite is higher (8.255 Å) than that of Fe^{2+}-rich chromite (cell size of 8.325 Å). Therefore, the development of porosity in chromite grains would be a result of the difference in molar volumes in chromite rather than in solubility effects. If so, the alteration of chromite grains would only took place where fluids were available. A temporal increase of the chromite porosity and permeability would happened, allowing the circulation of reducing and SiO_2-rich fluids and mobilizing MgO from the chromitite. Presence of SiO_2-rich fluids and the mobilization of MgO during retrograde metamorphism of ultramafic rocks (and enclosed chromitite ores) on the Tapo Ultramafic Massif is also suggested by the formation of scattered amphibolite lenses and carbonate-silica hydrothermalites (i.e., listwaenites and birbirites) filling thrust and faults in the ultramafic massif (Tassinari et al., 2011).

The volume of water necessary to produce the cited SiO_2-rich fluids can be estimated by comparing the silica content in the system before and after the alteration, which according to our computations varies from 9.60 wt% to 12 wt% (Fig. 8). Considering the minimum P-T conditions reached during greenschist-facies metamorphism (2.4 kbar and 300 °C; Willner et al., 2014) of the Tapo Ultramafic Massif, the volume of water necessary to dissolve 2.40 wt% SiO_2 in the forsterite + enstatite + H_2O system (Newton and Manning, 2002) is $9.15 \cdot 10^3$ cm^3. The circulation of this volume of fluids implies a 1:40 fluid/rock ratio, assuming that the density of unaltered semi-massive chromitite bodies (72:28 molar mix of cores of partly altered chromite and Fo_{92}) is 3.843 g/cm^3. It is very likely that the high fluid/rock ratio in semi-massive chromitite bodies might have enhanced the circulation of SiO_2-rich fluids and the mobilization of MgO, thus giving place to the chlorite + chromite assemblage predicted by our model and observed in partly altered chromite in semi-massive chromitites of the Tapo Ultramafic Massif.

6. Conclusions

(1) Two-stage, retrograde hydrous metamorphism in the Tapo Ultramafic Massif has produced chromite grains with three types of microstructures. In the first stage, the reaction between primary chromite and matrix olivine in presence of reducing and SiO_2-rich fluids resulted in the formation of Fe^{2+}-rich porous chromite rims (i.e., partly altered chromite), at high chromite/silicate ratio (72 vol% of chromite). At lower chromite/silicate ratios (<10 vol% of chromite) Fe-bearing fluids interacted with Fe^{2+}-rich porous chromite in serpentinites to form zoned and non-porous chromite grains.

(2) Based on the metamorphic zoning of chromite and the bulk composition of altered semi-massive chromitite we infer that the alteration of chromite was a dissolution-precipitation driven process. We modeled thermodynamically this reaction of alteration using hybrid chemical potential-bulk composition approach.

(3) μSiO_2-μMgO diagram calculated for the P-T conditions of the greenschist-facies overprint recorded in the studied area (i.e., 2 kbar and 300 °C) indicate that the transformation of the magmatic chromite to partly altered chromite (i.e., assemblage chromite + chlorite + eskolaite) took place at higher μSiO_2 (e.g., from −915 to −876 kJ/mol) but lower μMgO (e.g., from −598 to −579 kJ/mol) conditions. This indicates that the fluids that have produced the alteration were rich in SiO_2 but mobilized MgO out of the system. This can explain the presence of chlorite instead brucite in our samples.

(4) The careful application of P-T-X diagrams calculated according the different P-T pathways undergone by the chromitites and their enclosing metamorphic rocks confirm previous predictions that the alteration of chromitites took place under decreasing P and T conditions (i.e., retrograde

metamorphism), increasing SiO_2 and decreasing MgO content in the system. Modeled and natural metamorphic chromite shows identical compositional variations, which suggest that natural chromite does not preserve the record of the whole metamorphic pathway. Indeed, natural metamorphosed chromite only records the imprint of peak (either maximum or minimum) metamorphic conditions reached.

(5) In the chromitites from the Tapo Ultramafic Massif a high fluid/rock ratio (1:40 ratio), promoted by the circulation of reducing and SiO_2-rich fluids, was required to produce the observed microstructures and compositional changes in the chromitites. These fluids were derived from the dissolution of orthopyroxene and/or olivine from the host ultramafic rocks, whereas their releasing out from the chromitite produced the formation of garnet amphibolites and carbonate-silica hydrothermalites in the ultramafic massif.

Acknowledgements

This paper was supported by the project CGL2010-15171 and F. P.I. grant BES-2011-045423 of the Ministerio de Econonía y Competitividad (España). Support for this study has also been provided by the Fondecyt Intiation Grant #11140005 to J.M. González-Jiménez entitled "Decoding precious metals (platinum-group elements and gold) in upper mantle rocks of the Chilean Cordillera". J.M. González-Jiménez acknowledges funding by Ramón y Cajal Fellowship RYC-2015-17596 granted by the MINECO. The authors are particularly thankful to the editor Dr. Sisir Mondal and two anonymous reviewers for their constructive comments on the manuscript, which greatly improved the quality of the paper.

Appendix A. Supplementary data

Supplementary data associated with this article can be found, in the online version, at http://dx.doi.org/10.1016/j.oregeorev.2017.02.025.

References

Abzalov, M.Z., 1998. Chrome-spinels in gabbro-wehrlite intrusions of the Pechenga area, Kola Peninsula, Russia: emphasis on alteration features. Lithos 43 (3), 109–134.

Ahmed, A.H., Surour, A.A., 2016. Fluid-related modifications of Cr-spinel and olivine from ophiolitic peridotites by contact metamorphism of granitic intrusions in the Ablah area, Saudi Arabia. J. Asian Earth Sci. 122, 58–79.

Akmaz, R.M., Uysal, I., Saka, S., 2014. Compositional variations of chromite and solid inclusions in ophiolitic chromitites from the southeastern Turkey: implications for chromitite genesis. Ore Geol. Rev. 58, 208–224.

Bach, W., Paulick, H., Garrido, C.J., Ildefonse, B., Meurer, W.P., Humphris, S.E., 2006. Unraveling the sequence of serpentinization reactions: petrography, mineral chemistry, and petrophysics of serpentinites from MAR 15 N (ODP Leg 209, Site 1274). Geophys. Res. Lett. 33 (13), L13306.

Barnes, S.J., 2000. Chromite in komatiites, II. Modification during greenschist to mid-amphibolite facies metamorphism. J. Petrol. 41 (3), 387–409.

Barra, F., Gervilla, F., Hernández, E., Reich, M., Padrón-Navarta, J.A., González-Jiménez, J.M., 2014. Alteration patterns of chromian spinels from La Cabaña peridotite, south-central Chile. Miner. Petrol. 108 (6), 819–836.

Bliss, N.W., MacLean, W.H., 1975. The paragenesis of zoned chromite from central Manitoba. Geochim. Cosmochim. Acta 39 (6), 973–990.

Brenan, J.M., Rose, L.A., 2002. Experimental constraints on the wetting of chromite by sulfide liquid. Can. Mineral. 40 (4), 1113–1126.

Candia, M.A.F., Gaspar, J.C., 1997. Chromian spinels in metamorphosed ultramafic rocks from Mangabal I and II complexes, Goiás, Brazil. Mineral. Petrol. 60 (1), 27–40.

Cardona, A., Cordani, U.G., Sanchez, A., 2007. Metamorphic, geochronological and geochemical constraints from the Pre-Permian basement of the eastern Peruvian Andes (10○ S): a Paleozoic extensional-accretionary orogen. In: 20th Colloquium on Latin American Earth Sciences. Kiel, Germany, pp. 29–30.

Cardona, A., Cordani, U.G., Ruiz, J., Valencia, V.A., Armstrong, R., Chew, D.M., Nutman, A., Sanchez, A.W., 2009. U-Pb zircon geochronology and Nd isotopic signatures of the Pre-Mesozoic metamorphic basement of the Eastern Peruvian Andes: growth and provenance of a Late Neoproterozoic to Carboniferous accretionary orogen on the northwest margin of Gondwana. J. Geol. 117 (3), 285–305.

Castroviejo, R., Pereira, E., Rodrigues, J.F., Acosta, J., 2009. Pre-andean serpentinite-chromite orebodies in the Eastern Cordillera of Central Peru, Tarma province. In: Williams, P. (Ed.), Smart Science for Exploration and Mining: Proceedings of the 10th Biennial SGA Meeting. Economic Geology Research Unit James Cook University, Townsville, Australia, pp. 927–929.

Chatterjee, N.D., Leistner, H., Terhart, L., Abraham, K., Klaska, R., 1982. Thermodynamic mixing properties of corundum-eskolaite, α-(Al, Cr^3)$_2O_3$, crystalline solutions at high temperatures and pressures. Am. Mineral. 67 (7–8), 725–735.

Chew, D.M., Schaltegger, U., Miškovic, A., Fontignie, D., Frank, M., 2005. Deciphering the tectonic evolution of the Peruvian segment of the Gondwanan margin. In: Proceedings of the 6th International Symposium on Andean Geodynamics. Institut de recherche pour le développement, Spain, Barcelona, pp. 166–169.

Chew, D.M., Schaltegger, U., Košler, J., Whitehouse, M.J., Gutjahr, M., Spikings, R.A., Miškovic, A., 2007. U-Pb geochronologic evidence for the evolution of the Gondwanan margin of the north-central Andes. Geol. Soc. Am. Bull. 119 (5–6), 697–711.

Colás, V., González-Jiménez, J.M., Griffin, W.L., Fanlo, I., Gervilla, F., O'Reilly, S.Y., Pearson, N.J., Kerestedjian, T., Proenza, J.A., 2014. Fingerprints of metamorphism in chromite: new insights from minor and trace elements. Chem. Geol. 389, 137–152.

Connolly, J.A.D., 2009. The geodynamic equation of state: what and how. Geochem. Geophys. Geosyt. 10 (10), Q10014.

Dalmayrac, B., Laubacher, G., Marocco, R., 1980. Geologie des Andes Peruviénnes. Caractéres generaux de l'evolucion geologique des Andes Peruviénnes. ed. Travaux et document de l'Office de La Recherchè Scientifique et Technique Outre-mer, Paris.

Dick, H.J.B., Bullen, T., 1984. Chromian spinel as a petrogenetic indicator in abyssal and alpine-type peridotites and spatially associated lavas. Contrib. Mineral. Petrol. 86 (1), 54–76.

Droop, G.T.R., 1987. A general equation for estimating Fe^{3+} concentrations in ferromagnesian silicates and oxides from microprobe analyses, using stoichiometric criteria. Mineral. Mag. 51 (361), 431–435.

Engi, M., 1983. Equilibria involving Al-Cr spine: Mg-Fe exchange with olivine. Experiments, thermodynamic analysis, and consequences for geothermometry. Am. J. Sci. 284-A (3), 29–71.

Evans, D.M., 2015. Metamorphic modifications of the Muremera mafic–ultramafic intrusions, eastern Burundi, and their effect on chromite compositions. J. Afr. Earth Sci. 101, 19–34.

Evans, B.W., Frost, B.R., 1975. Chrome-spinel in progressive metamorphism- A preliminary analysis. Geochim. Cosmochim. Acta 39 (6–7), 959–972.

Evans, K.A., Powell, R., Frost, B.R., 2013. Using equilibrium thermodynamics in the study of metasomatic alteration, illustrated by an application to serpentinites. Lithos 168–169, 67–84.

Fleet, M.E., Angeli, N., Pan, Y., 1993. Oriented chlorite lamellae in chromite from the Pedra Branca mafic-ultramafic complex, Ceara, Brazil. Am. Mineral. 78 (1–2), 68–74.

Frost, B.R., Beard, J.S., 2007. On silica activity and serpentinization. J. Petrol. 48 (7), 1351–1368.

Frost, B.R., Evans, K.A., Swapp, S.M., Beard, J.S., Mothersole, F.E., 2013. The process of serpentinization in dunite from New Caledonia. Lithos 178, 24–39.

Gahlan, H.A., Azer, M.K., Khalil, A.E.S., 2015. The Neoproterozoic Abu Dahr ophiolite, South Eastern Desert, Egypt: petrological characteristics and tectonomagmatic evolution. Miner. Petrol. 109 (5), 611–630.

Gargiulo, M.F., Bjerg, E.A., Mogessie, A., 2013. Spinel group minerals in metamorphosed ultramafic rocks from Río de Las Tunas belt, Central Andes, Argentina. Geol. Acta 11 (2), 133–148.

Gervilla, F., Padrón-Navarta, J.A., Kerestedjian, T., Sergeeva, I., González-Jiménez, J. M., 2012. Formation of ferrian chromite in podiform chromitites from the Golyamo Kamenyane serpentinite, Eastern Rhodopes, SE Bulgaria: a two-stage process. Contrib. Mineral. Petrol. 164 (4), 643–657.

González-Jiménez, J.M., Kerestedjian, T., Proenza, J.A., Gervilla, F., 2009. Metamorphism on chromite ores from the Dobromirtsi ultramafic massif, Rhodope Mountains (SE Bulgaria). Geol. Acta 7 (4), 413–429.

González-Jiménez, J.M., Reich, M., Camprubí, A., Gervilla, F., Griffin, W.L., Colás, V., O'Reilly, S.Y., Proenza, J.A., Pearson, N.J., Centeno-García, E., 2015. Thermal metamorphism of mantle chromites and the stability of noble-metal nanoparticles. Contrib. Mineral. Petrol. 170 (2), 1–20.

González-Jiménez, J.M., Barra, F., Garrido, L.N.F., Reich, M., Satsukawa, T., Romero, R., Salazar, E., Colás, V., Orellana, F., Rabbia, O., Plissart, G., Morata, D., 2016. A secondary precious and base metal mineralization in chromitites linked to the development of a Paleozoic accretionary complex in Central Chile. Ore Geol. Rev. 78, 14–40.

Holland, T.J.B., Powell, R., 1998. An internally consistent thermodynamic data set for phases of petrological interest. J. Metamorphase Geol. 16 (3), 309–343.

Jöns, N., Bach, W., Klein, F., 2010. Magmatic influence on reaction paths and element transport during serpentinization. Chem. Geol. 274 (3), 196–211.

Kamenetsky, V.S., Gurenko, A.A., 2007. Cryptic crustal contamination of MORB primitive melts recorded in olivine-hosted glass and mineral inclusions. Contrib. Mineral. Petrol. 153 (4), 465–481.

Kimball, K.L., 1990. Effects of hydrothermal alteration on the compositions of chromian spinels. Contrib. Mineral. Petrol. 105 (3), 337–346.

Klemme, S., Ivanic, T.J., Connolly, J.A.D., Harte, B., 2009. Thermodynamic modelling of Cr-bearing garnets with implications for diamond inclusions and peridotite xenoliths. Lithos 112, 986–991.
Kotschoubey, B., Villas, R.N., Aires, B., 2016. Chloritites of the Tocantins Group, Araguaia fold belt, central-northern Brazil: vestiges of basaltic magmatism and metallogenetic implications. J. South. Am. Earth. Sci. 69, 171–193.
Leblanc, M., Nicolas, A., 1992. Ophiolitic chromitites. Int. Geol. Rev. 34 (7), 653–686.
Lenaz, D., Braidotti, R., Princivalle, F., Garuti, G., Zaccarini, F., 2007. Crystal chemistry and structural refinement of chromites from different chromitite layers and xenoliths of the Bushveld Complex. Eur. J. Mineral. 19 (4), 599–609.
Loferski, P.J., 1986. Petrology of Metamorphosed Chromite-Bearing Ultramafic Rocks From the Red Lodge District, Montana. U.S. Government Printing Office, Alexandria, USA.
Majumdar, A.S., Hövelmann, J., Vollmer, C., Berndt, J., Mondal, S.K., Putnis, A., 2016. Formation of Mg-rich olivine pseudomorphs in serpentinized dunite from the Mesoarchean Nuasahi Massif, Eastern India: insights into the eevolution of fluid composition at the mineral-fluid interface. J. Petrol. 57 (1), 3–26.
Megard, F., Caldas, J., Paredes, V.J., Cruz, N., 1996. Geología de los cuadrángulos de Tarma, La Oroya y Yauyos (Memoria). ed. INGEMMET, Lima.
Merlini, A., Grieco, G., Diella, V., 2009. Ferritchromite and chromian-chlorite formation in mélange-hosted Kalkan chromitite (Southern Urals, Russia). Am. Mineral. 94 (10), 1459–1467.
Mukherjee, R., Mondal, S.K., Rosing, M.T., Frei, R., 2010. Compositional variations in the Mesoarchean chromites of the Nuggihalli schist belt, Western Dharwar Craton (India): potential parental melts and implications for tectonic setting. Contrib. Mineral. Petrol. 160 (6), 865–885.
Mukherjee, R., Mondal, S.K., González-Jiménez, J.M., Griffin, W.L., Pearson, N.J., O'Reilly, S.Y., 2015. Trace-element fingerprints of chromite, magnetite and sulfides from the 3.1 Ga ultramafic–mafic rocks of the Nuggihalli greenstone belt, Western Dharwar craton (India). Contrib. Mineral. Petrol. 169 (6), 1–23.
Newton, R.C., Manning, C.E., 2002. Solubility of enstatite + forsterite in H_2O at deep crust/upper mantle conditions: 4 to 15 kbar and 700 to 900 °C. Geochim. Cosmochim. Acta 66 (23), 4165–4176.
Oka, Y., Steinke, P., Chatterjee, N.D., 1984. Thermodynamic mixing properties of Mg (Al, Cr)2O4 spinel crystalline solution at high temperatures and pressures. Contrib. Mineral. Petrol. 87 (2), 196–204.
Oze, C., Fendorf, S., Bird, D.K., Coleman, R.G., 2004. Chromium geochemistry in serpentinized ultramafic rocks and serpentine soils from the Franciscan complex of California. Am. J. Sci. 304 (1), 67–101.
Polat, A., Herzberg, C., Münker, C., Rodgers, R., Kusky, T.M., Li, J., Fryer, B., Delaney, J., 2006. Geochemical and petrological evidence for a suprasubduction zone origin of Neoarchean (ca. 2.5 Ga) peridotites, central orogenic belt, North China craton. Geol. Soc. Am. Bull. 118 (7–8), 771–784.
Prabhakar, N., Bhattacharya, A., 2013. Origin of zoned spinel by coupled dissolution–precipitation and inter-crystalline diffusion: evidence from serpentinized wehrlite, Bangriposi, Eastern India. Contrib. Mineral. Petrol. 166 (4), 1047–1066.
Proenza, J.A., Gervilla, F., Melgarejo, J.C., Bodinier, J.L., 1999. Al-and Cr-rich chromitites from the Mayarí-Baracoa ophiolitic belt (eastern Cuba); consequence of interaction between volatile-rich melts and peridotites in suprasubduction mantle. Econ. Geol. 94 (4), 547–566.
Proenza, J.A., Ortega-Gutiérrez, F., Camprubí, A., Tritlla, J., Elías-Herrera, M., Reyes-Salas, M., 2004. Paleozoic serpentinite-enclosed chromitites from Tehuitzingo (Acatlán Complex, southern Mexico): a petrological and mineralogical study. J. South. Am. Earth. Sci. 16 (8), 649–666.
Putnis, A., 2002. Mineral replacement reactions: from macroscopic observations to microscopic mechanisms. Mineral. Mag. 66 (5), 689–708.
Putnis, A., 2009. Mineral replacement reactions. Rev. Mineral. Geochem. 70 (1), 87–124.
Putnis, A., 2015. Transient porosity resulting from fluid–mineral interaction and its consequences. Rev. Mineral. Geochem. 80, 1–23.
Putnis, A., Austrheim, H., 2010. Fluid-induced processes: metasomatism and metamorphism. Geofluids 10 (1–2), 254–269.
Rasband, W.S., 2007. Image J. In: Bethesda, M.D. (Ed.). US National Institutes of Health.
Satsukawa, T., Piazolo, S., González-Jiménez, J.M., Colás, V., Griffin, W.L., O'Reilly, S. Y., Gervilla, F., Fanlo, I., Kerestedjian, T., Kerestedjian, T., 2015. Fluid-present deformation aids chemical modification of chromite: insights from chromites from Golyamo Kamenyane, SE Bulgaria. Lithos 228, 78–89.
Saumur, B.M., Hattori, K., 2013. Zoned Cr-spinel and ferritchromite alteration in forearc mantle serpentinites of the Rio San Juan Complex. Dominican Republic. Mineral. Mag. 77 (1), 117–136.
Tassinari, C.C.G., Castroviejo, R., Rodrigues, J.F., Acosta, J., Pereira, E., 2011. A Neoproterozoic age for the chromitite and gabbro of the Tapo ultramafic Massif, Eastern Cordillera, Central Peru and its tectonic implications. J. South. Am. Earth. Sci. 32 (4), 429–437.
Tian, W., Chen, B., Ireland, T.R., Green, D.H., Suzuki, K., Chu, Z., 2011. Petrology and geochemistry of dunites, chromitites and mineral inclusions from the Gaositai Alaskan-type complex, North China Craton: implications for mantle source characteristics. Lithos 127 (1), 165–175.
Ulmer, G.C., 1974. Alteration of chromite dring serpentinization the Pennsylvania-Maryland District. Am. Mineral. 59, 1236–1241.
Whitney, D.L., Evans, B.W., 2010. Abbreviations for names of rock-forming minerals. Am. Mineral. 95 (1), 185–187.
Willner, A.P., Tassinari, C.C.G., Rodrigues, J.F., Acosta, J., Castroviejo, R., Rivera, M., 2014. Contrasting Ordovician high-and low-pressure metamorphism related to a microcontinent-arc collision in the Eastern Cordillera of Perú (Tarma province). J. South. Am. Earth. Sci. 54, 71–81.
Wilson, J., Reyes, L., 1964. Geología del Cuadrángulo de Pataz. Boletín serie a 9. Escala 1:100,000. ed. Instituto Geológico Minero y Metalúrgico, Carta Geológica Nacional, Lima.
Zaccarini, F., Pushkarev, E., Garuti, G., 2008. Platinum-group element mineralogy and geochemistry of chromitite of the Kluchevskoy ophiolite complex, central Urals (Russia). Ore Geol. Rev. 33 (1), 20–30.